

Entropy stabilization effects and ion migration in 3D “hollow” halide perovskites

K. Jayanthi¹, Ioannis Spanopoulos^{2,3}, Nourdine Zibouche⁴, Albert A. Voskanyan¹ Eugenia S. Vasileiadou², M. Saiful Islam^{*4,5}, Alexandra Navrotsky^{*1} and Mercuri G. Kanatzidis^{*2}

¹*School of Molecular Sciences and Navrotsky Eyring Center for Materials of the Universe, Arizona State University, Tempe, Arizona 85287, USA*

²*Department of Chemistry, Northwestern University, Evanston, Illinois 60208, USA*

³*Department of Chemistry, University of South Florida, Tampa, Florida 33620, USA*

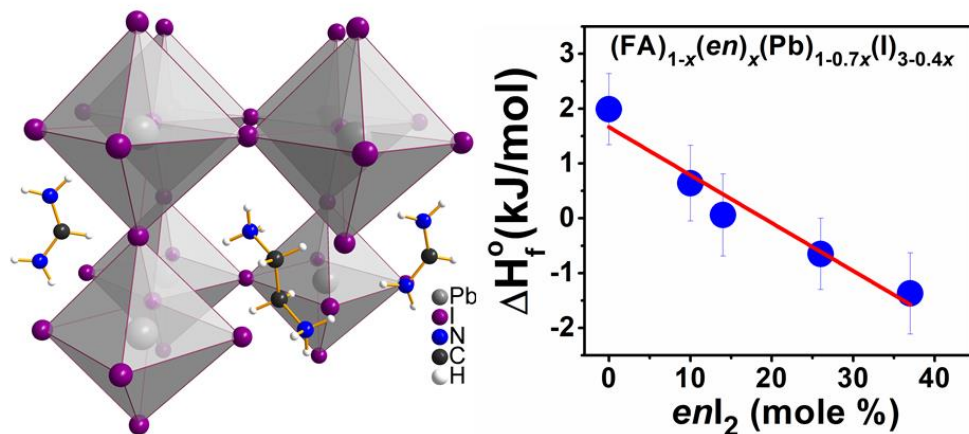
⁴*Department of Chemistry, University of Bath, Bath BA2 7AY, UK*

⁵*Department of Materials, University of Oxford, Oxford OX1 3PH, UK*

Abstract: A recently discovered new family of 3D halide perovskites with the general formula $(A)_{1-x}(en)_x(Pb)_{1-0.7x}(X)_{3-0.4x}$ ($A = MA, FA$; $X = Br, I$; $MA =$ methylammonium, $FA =$ formamidinium, $en =$ ethylenediammonium) is referred to as “hollow” perovskites owing to extensive Pb, and X vacancies created on incorporation of en cations in the 3D network. The “hollow” motif allows fine tuning of optical, electronic, and transport properties, as well as bestowing good environmental stability proportional to en loading. To shed light on the origin of the apparent stability of these materials we performed detailed thermochemical studies, using room temperature solution calorimetry combined with density functional theory simulations on three different families of “hollow” perovskites namely $en/FAPbI_3$, $en/MAPbI_3$ and, $en/FAPbBr_3$. We found that the bromide perovskites are more energetically stable compared to iodide perovskites in the FA- based hollow compounds, as shown by the measured enthalpies of formation and the calculated formation energies. The least stable $FAPbI_3$ gains stability on incorporation of the en

cation, whereas FAPbBr_3 becomes less stable with *en* loading. This behavior is attributed to the difference in the 3D cage size in the bromide and iodide perovskites. Configurational entropy, which arise from randomly distributed cation and anion vacancies, play a significant role in stabilizing these “hollow” perovskite structures despite small differences in their formation enthalpies. With the increased vacancy defect population, we have also examined halide ion migration in the FA-based “hollow” perovskites and found that the migration energy barriers become smaller with increasing *en* content.

TABLE OF CONTENTS GRAPHIC



1. INTRODUCTION

Hybrid halide perovskites are promising semiconductors for the development of next generation photovoltaic technologies owing to their versatile structural nature and unique combination of optoelectronic and mechanical traits.¹⁻⁴ The range of features include tunable energy band gaps, high absorption coefficients, high defect tolerance, long carrier diffusion lengths, low Young's modulus and solution processability.⁵⁻⁹ Recently, a record PCE of 25.5% was achieved,¹⁰ which is comparable to current commercially available technologies based on GaAs, CdTe and Si.¹¹⁻¹⁵ However, the poor environmental stability upon exposure to air, light and heat impairs the device performance and hence reduces the recorded PCEs, which hinders their commercialization.¹⁶ Hence, tremendous research efforts are devoted towards solving the instability issues by focusing either on optimizing the device assembly architecture and/or on developing new perovskite materials with enhanced environmental stability.¹⁷⁻²¹

Halide perovskite materials exhibiting the three-dimensional (3D) perovskite structure have a general formula of ABX_3 (A= MA, FA, and Cs; B = Pb, Sn, and Ge; X = Cl, Br, and I). This structure consists of corner sharing BX_6 metal halide octahedra with A site counter cations occupying the cuboctahedral cages.^{22,23} The most exploited 3D halide perovskites are the pristine $FAPbI_3$ and $MAPbI_3$ as well as materials that are based on combinations of halides and mixed A site cations, such as $(MA_xFA_{1-x})Pb(I_yBr_{3-y})$, which have proven to be the best choice for the assembly of highly efficient perovskite solar cells.²⁴⁻²⁷ The intrinsic stability of hybrid halide perovskite depends on choice of the organic cation and their formation energies.^{1, 28-35}

Recently, we reported a new family of 3D-hybrid halide perovskites, which are highly defective yet crystalline, termed "hollow" perovskites, with a general formula of $(A)_{1-x}(en)_x(M)_{1-0.7x}(X)_{3-0.4x}$ (A = MA, FA; M = Pb, Sn; X = Br, I; $0 < x \leq 0.48$).³⁶⁻³⁹ The incorporation of the large

ethylenediammonium (*en*) dication in the ABX_3 structure deviates significantly from Goldschmidt's tolerance factor rules,⁴⁰ which appear essential for the stabilization of the 3D perovskites. Despite this, the perovskite structure accommodates *en* in the cuboctahedral cage by replacing the A cation and by a partial removal of B and X atoms from the ABX_3 crystal structure. These newly assembled “hollow” perovskites conserve their isotropic 3D structure despite high defect densities.³⁶⁻³⁹ The “hollow” strategy allows fine-tuning of the properties of the corresponding materials, including absorption and emission spectra as well as their electronic and ionic conductivities. In addition to these merits, hollowness bestows exceptional air stability to the synthesized materials.

To shed light on the reasons behind the apparent high air stability of this unique class of perovskite semiconductors, in a previous study³⁷ we performed DC polarization experiments and DFT calculations on the *en*/MAPbI₃ system. The results showed an increase of the activation energy for iodide ion migration and higher relaxation times of the iodine gas/solid exchange with increasing amount of *en* in the “hollow” structure.³⁷ Although these features provide information about the kinetic stability of the corresponding materials, there is no information on the thermodynamic stability so far.

To elucidate the thermodynamic stability, in this work we performed extensive thermochemical studies, using room temperature solution calorimetry, to identify the thermodynamic properties of three different families of “hollow” perovskites, namely, %*en*/FAPbI₃, %*en*/MAPbI₃ and %*en*/FAPbBr₃ where % means mole percent. Due to the intrinsic issue of defect-mediated ion migration, we also used *ab initio* simulation methods to examine trends in ion migration activation energies in these “hollow” perovskites at the atomic level. We identified the effect of *en* addition on the thermodynamic stability of these materials, as well as

the differences in the measured dissolution enthalpies and the calculated formation enthalpies between the iodide and bromide materials. We found that the FA-based bromide perovskites are more stable than their iodide perovskites. The metastable FAPbI₃ gains stability on incorporation of the *en* cation, whereas the bromide system FAPbBr₃ becomes less stable. This behavior is attributed to the difference in the 3D cage size in the bromide and iodide perovskite structures. Configurational entropy, which arises from randomly dispersed cation and anion vacancies, plays a significant role in stabilizing these “hollow” perovskite structures despite small difference in their formation enthalpies.

2. RESULTS AND DISCUSSION

2.1 Structural characterization

Using previously established synthetic protocols (see SI), three different families of “hollow” perovskite single crystals were synthesized, namely the (FA)_{1-x}(*en*)_x(Pb)_{1-0.7x}(I)_{3-0.4x} iodide series with *en* loading $x = 0.0, 0.10, 0.14, 0.26, 0.37$, the (FA)_{1-x}(*en*)_x(Pb)_{1-0.7x}(Br)_{3-0.4x} bromide series with *en* amount $x = 0.0, 0.07, 0.14, 0.23, 0.38$, and the (MA)_{1-x}(*en*)_x(Pb)_{1-0.7x}(I)_{3-0.4x} iodide series with *en* loading $x = 0.0, 0.13, 0.25, 0.48$. For simplicity, the following notation will be utilized throughout this work: %*en*/FAPbI₃, %*en*/MAPbI₃ and %*en*/FAPbBr₃ to refer to (FA)_{1-x}(*en*)_x(Pb)_{1-0.7x}(I)_{3-0.4x}, (MA)_{1-x}(*en*)_x(Pb)_{1-0.7x}(I)_{3-0.4x}, (FA)_{1-x}(*en*)_x(Pb)_{1-0.7x}(Br)_{3-0.4x}, respectively. A schematic crystal structure of the 3D “hollow” perovskites is shown in Figure 1. Powder X-ray diffraction (PXRD) studies validated the phase purity of the synthesized materials (Figures S1-7). Additional signature characteristics of the “hollow” materials is the unit cell expansion upon *en* inclusion, which is evident by the shift of the diffraction patterns to lower 2θ values, in addition to the structural phase transitions among the cubic (α phase) and tetragonal (β phase) perovskite phases (Figure 2, S3-5). It is clear that the %*en*/FAPbI₃ ($0 < en \leq 14$) compounds

are isostructural to cubic α -FAPbI₃, (space group $Pm\bar{3}m$) (Figure 2).³⁸ There are additional diffraction peaks observed at $2\theta = 22.3^\circ$ and 26.4° for $x \geq 26\%$, that are characteristic of the formation of a pure tetragonal β -phase of FAPbI₃, (space group $P4/mbm$). In contrast, the family of $\%en$ /MAPbI₃ for $en \leq 13\%$ is isostructural to the tetragonal β phase of MAPbI₃ (space group $I4/mcm$), while for $en > 25\%$, the materials crystallize in the cubic α phase MAPbI₃ (space group $Pm\bar{3}m$)(Figure S3).³⁰ Notably, all $\%en$ FAPbBr₃ compounds are isostructural to the pristine cubic α -FAPbBr₃ (space group $Pm\bar{3}m$); there are no observed phase transitions with en loading for the bromide perovskites (Figure S6).³⁹

The presence of en molecular cations in the crystal structure and the corresponding en fraction for each composition were verified and determined by ¹H-NMR spectroscopy (see SI). The dried crystals were dissolved in DMSO-d₆ and the cations ratios were determined by integrating their NMR peak signatures. For en /MAPbI₃ perovskites the quantification is based on both the methyl (-CH₃, $\delta = 2.38$ ppm) and the ammonium (-NH₃⁺, $\delta = 7.49$ ppm) protons of the methylammonium cation versus the methylene (-CH₂-, $\delta = 3.02$ ppm) and the ammonium (-NH₃⁺, $\delta = 7.77$ ppm) protons of the en cations. The integration of MA peaks reveals a ratio of 1:1, since there are three protons from the methyl group (-CH₃) and three protons from the amine cation (-NH₃⁺) (Figures S8-10). For en /FAPbI₃ and en /FAPbBr₃ perovskites the quantification was based on both the methine (=CH-, $\delta = 7.87$ ppm) and the ammonium (-NH₂⁺, $\delta = 8.64$ ppm, 9.00 ppm) protons of the FA cation versus the methylene (-CH₂-, $\delta = 3.02$ ppm) and the ammonium (-NH₃⁺, $\delta = 7.77$ ppm) protons of the en cations. In FA, the integration of the proton peaks reveals a ratio of 2:2:1, since there is one proton from the methine group (=CH-) and four protons from the two amine cations (-NH₂⁺)(Figures S11-18). In en , the ratio of the 2 peaks is 4:6, arising from four (-CH₂-) protons and six ammonium (-NH₃⁺) protons, suggesting that en is doubly protonated.

2.2 Energetics of *en* incorporation from calorimetry measurements

Room temperature solution calorimetry measurements were performed to investigate the energetic impact of *en* incorporation in %*en*/APbX₃ (A = FA, MA; X = Cl, Br) “hollow” perovskites and its impact on the dissolution enthalpies (ΔH_{ds}) and formation enthalpy (ΔH°_f) values (for detailed description of the calorimetry measurements, see SI). The thermochemical cycle used to calculate the ΔH°_f is given in Table 1. The measured ΔH_{ds} and the resulting ΔH°_f from binary halide components are listed in Table S1. The variation of ΔH°_f and ΔH_{ds} of the “hollow” perovskites as a function of *en*X₂ (X = I, Br) are plotted in Figure 3 and Figure S19, respectively. The ΔH_{ds} energies as a function of %*en* follow linear trends for both %*en*/FAPbI₃, and %*en*/FAPbBr₃ “hollow” perovskites (Figure S19). However, the values become less exothermic with the increase of *en* content in the perovskite structure. The ΔH_{ds} values for %*en*/FAPbI₃ are more exothermic varying from -78.92 ± 0.42 to -73.37 ± 0.45 kJ/mol compared to %*en*/FAPbBr₃ perovskites, which vary from -54.57 ± 0.33 to -51.31 ± 0.39 kJ/mol (Table S1, and Figure S19). Consequently, the formation enthalpies, ΔH°_f , of %*en*/FAPbBr₃ perovskites are more exothermic compared to %*en*/FAPbI₃ upon incorporation of *en*, as shown in Table S1, and Figure 3. ΔH_{ds} and ΔH°_f indicates that the %*en*/FAPbBr₃ perovskites are energetically more stable than %*en*/FAPbI₃. These results are commensurate with the literature reports on hybrid halide perovskites, confirming the increase in the thermodynamic instability with larger halide anions.¹ The values of ΔH°_f in Table S1 show that the incorporation of *en* results in more stable %*en*/FAPbI₃ compared to metastable pristine FAPbI₃, whereas, the %*en*/FAPbBr₃ systems become less stable than pristine FAPbBr₃.³⁶⁻³⁹ To obviate any possible solvent-precursor and precursor-precursor interactions in the DMSO solvent that could have an impact on the ΔH_{ds} and ΔH°_f values mechanical mixtures of binary components were investigated (see SI, Table S2, S3).

This difference in the stability trends between %*en*/FAPbI₃ and %*en*/FAPbBr₃ systems upon incorporation of *en* can be attributed to the different sizes of the halide ions (I and Br) and hence the 3D cage formed by PbX₆ framework in the perovskite structures. In %*en*/FAPbI₃, the 3D cage is larger and can easily accommodate the *en* dication molecules, compared to the cage in the %*en*/FAPbBr₃, and the structure endures a local strain upon incorporation of *en* in place of FA cations. The increase of *en* content produces an increase in the strain and hence raises the internal energy of the perovskite structure, which consequently causes %*en*/FAPbBr₃ to become less stable with increasing *en* content. Consequently, ΔH°_f of the bromide perovskites between 0%*en* to 38%*en* become less exothermic, with energies varying from -5.60 ± 0.55 kJ/mol to -1.57 ± 0.50 kJ/mol. Meanwhile, ΔH°_f of the iodide perovskites between 0%*en* to 38%*en* become more exothermic, as the energies vary from 1.99 ± 0.65 kJ/mol to -1.37 ± 0.74 kJ/mol.

To further complement our findings, we have used density functional theory (DFT) methods to compute the formation energies (E_f) of the %*en*/APbX₃ perovskites relative to their pristine materials (without *en*) for *en* concentrations of 6.25% and 37.5% (details of the calculations at zero K are provided in the SI). The formation energies of the %*en*/FAPbI₃ systems are 1.03 kJ/mol and 2.59 kJ/mol higher than that of the pristine FAPbI₃ for 6.25% and 37.5% *en* content, respectively. In the case of %*en*/FAPbBr₃ perovskites, the formation energies are 2.02 kJ/mol and 5.00 kJ/mol higher than their pristine FAPbBr₃ for *en* concentrations of 6.25% and 37.5%, respectively. Overall, for the FA-based “hollow” perovskites, our calculated formation energies are in a good agreement with the experimental formation enthalpies. In the case of %*en*/FAPbBr₃, the closest experimental *en* concentrations to the computational *en* values are 7% and 38% *en*. The difference in the formation enthalpies of the latter concentrations relative to their pristine FAPbBr₃ (0%*en*) are 0.51 kJ/mol and 4.03 kJ/mol (Table S1), which agree with our

computed values for the 6.25 and 37.5% concentrations within the experimental errors. These results show that the energetic stability for the %*en*/FAPbBr₃ systems become less exothermic with increase of *en* content. For %*en*/FAPbI₃ perovskites, the closest corresponding experimental compounds to our modeled systems are 10% and 37%*en*, their formation enthalpies differ by 1.35 kJ/mol and 3.56 kJ/mol compared to the pristine FAPbI₃. These values are also consistent with the computed formation energy differences of the corresponding systems 6.25% and 37.5%*en* within the experimental error.

The %*en*/MAPbI₃ perovskites do not follow any discernible trend in the ΔH_{ds} and ΔH°_f for different *en* concentrations. The dissolution enthalpies are about ~ -73 kJ/mol and the corresponding formation enthalpies are around ~ 1 kJ/mol, as shown in Table S1. It should be noted that although the differences in ΔH_{ds} and ΔH°_f are small in magnitude, ranging from +2 to -6 kJ/mol, among %*en*/FAPbX₃ perovskites, they still follow a linear trend. Thermodynamic stability comes from the combination of enthalpy and entropy factors. Energetics arise from factors like size difference, orientation mismatch, linker topology, and electronic effects. These factors cannot be separated based on thermochemistry, as all contribute to the measured enthalpies. Opposing competing factors can cancel each other. Considering the observation that ΔH°_f may does not depend strongly on *en* incorporation in the hollow perovskites (%*en*/(FA/MA)PbX₃), the entropy and kinetic stability may play key roles, as we have shown in the previous study on ion migration of iodide anions in the hollow MAPbI₃ structures.³⁷

The computed formation energies of the %*en*MAPbI₃ systems relative to their pristine MAPbI₃ are 1.15 and 2.36 kJ/mol higher for the 6.25% and 37.5% *en* contents, which are also comparable to the corresponding experimental formation enthalpies. The small variations of the formation enthalpies and the calculated formation energies of %*en*MAPbI₃ perovskites indicate

that the stability of MAPbI₃ is not significantly affected when *en* is incorporated. The difference in the “exothermicity” trends between %*en*MAPbI₃ and %*en*FAPbI₃ perovskites could be explained by the size difference of MA and FA cations in addition to the tetragonal and cubic systems in which they crystallize at room temperature. Essentially, the hosting 3D cage of the A-site cation is larger for FA than MA. Moreover, the tetragonal system has one stretched and two shortened lattice constants compared to the cubic phase. This means that when MA is substituted by *en*, the latter will likely to accommodate itself along the elongated direction and will experience a compressive strain along the two shortened directions. This induced strain causes an increase in the internal energy of the system and hence results in less exothermic %*en*MAPbI₃ compounds compared to %*en*FAPbI₃ counterparts.

Entropy plays a significant role in stabilizing these “hollow” perovskites. Configurational entropy arises from randomly dispersed cation and anion vacancies creating hollowness in the 3D “hollow” perovskites. Assuming a random mixing of FA/MA and *en* cations in the A site, Pb atoms and vacancies in the B site, halide anions and the vacancies in the X site, we calculated the configurational entropy (S_{conf}) contributions from published metal occupancies in these sites (see SI).^{38,39} Disorder, or hollowness increases with increasing *en* amounts in the perovskite structure and so does the S_{conf} . It is zero for the pristine systems (i.e. 0%*en*), and increases linearly with *en* content to 11.87 J/mol/K for 37%*en*/FAPbI₃, to 12.00 J/mol/K for 38%*en*/FAPbBr₃, and to 13.04 J/mol/K for 48%*en*/MAPbI₃ (Table S1). The ability to stabilize the perovskite compounds with this level of configurational disorder offers new avenues for designing entropy-stabilized perovskite structures. Configurational entropy arising from disordered cation and anion distributions results in a remarkable stabilization of otherwise energetically metastable mixed metal halide perovskites. Multiple halide ions (I, Br, and Cl) in the X site and/or cations (MA, FA,

GA, and Cs) in the A site of the ABX_3 perovskite structure may generate new and more stable perovskites with unique physicochemical properties.⁴¹⁻⁴⁴ In addition, the role of vibrational entropy needs to be better understood to give a more complete picture of entropy contributions in these “hollow” perovskites, but it is beyond the scope of this paper.

In making the “hollow” perovskites, just enough hollowness is created to form a marginally stable material, thus making its formation possible. The inclusion of *en* and exclusion of Pb and X from the perovskite structure involve bond breaking and bond making processes. The energy lost during exclusion of Pb and X which involves a bond breaking process is compensated by the inclusion of *en*, which involves the formation of new hydrogen bonds with *en*. Thus, balancing of the total energy could be the driving the formation of “hollow” perovskites.

2.3 Computed energetics of ion migration in “hollow” perovskites

In addition to thermodynamic stability, ion migration mediated by anion vacancy defects may be an inherent stability issue in “hollow” perovskites, and hence it is important to understand such transport properties especially at the atomic level. We have previously shown that the activation energies of migrating iodide vacancies increase with *en* content in “hollow” %*en*/MAPbI₃ perovskites.³⁷ In this study, we have also calculated the activation energies for halide (I, Br) ion migration of the corresponding %*en*/FAPbX₃ compounds. As in our previous study, we have simulated two *en* contents of 6.25% and 37.5% for comparison (Computational methods are provided in the SI, which have been applied successfully to studies of ion migration and A-cation effects in other perovskite halides.^{37,45-48}

First, the simulations of the “hollow” perovskite structures support the structural characterization in which the divalent *en* cation substitutes the A-cation (MA, FA) and a Pb²⁺ ion,

with charge-compensation by anion vacancies. Such defect chemistry would support anion vacancy-mediated ion migration. We have considered four migration pathways within the same PbX_6 octahedron. These pathways share the same initial anion vacancy, VI or VBr, and are designated as VI→V1 and VI→V2 along the equatorial direction and as VI→V3 and VI→V4 along the apical direction, as shown in Figure 4. Although we recognize that other paths are possible, the numerous paths examined near the *en* cation provides valuable trends in activation energies, which is the main focus here. The activation energies for each path are given in Table S4.

For long-range ion migration, we discuss the overall mean values of the activation energies for each concentration in the %*en*/FAPbX₃ perovskites. For the migration pathways in 6.25% *en*, the mean activation energies are 0.48 eV (46.31 kJ/mol) and 0.36 eV (34.74 kJ/mol) for %*en*/FAPbI₃ and %*en*/FAPbBr₃, respectively. The values for the higher *en* content of 37.5% are 0.38 eV (36.66 kJ/mol) and 0.26 eV (25.09 kJ/mol) for %*en*/FAPbI₃ and %*en*/FAPbBr₃, respectively. These results show that the activation energy barriers in %*en*/FAPbBr₃ are smaller than those in %*en*/FAPbI₃. This could be explained by the difference in I/Br ion size and shorter Pb-Br bond-lengths and hence shorter migration paths in the bromide systems compared to the iodide counterparts. We note that this small difference in the migration energy barriers between %*en*/FAPbI₃ and %*en*/FAPbBr₃ perovskites may be one of the possible factors related to less exothermic %*en*/FAPbBr₃ compared to %*en*/FAPbI₃ with increasing *en* content, as discussed above. Interestingly, unlike %*en*/MAPbI₃ perovskites, the activation energies in %*en*/FAPbX₃ decrease with increasing *en* content from 6.25 to 37.5%, irrespective of the halide anion. While in %*en*/MAPbI₃ the mean activation energy increases from 0.56 eV (54.03 kJ/mol) at 6.25% *en* to 0.69 eV (92.63 kJ/mol) at 37.5% *en*.³⁷

From analysis of the simulated structures, we did not find any clear differences in the inherent perovskite framework and lattice distortion between MA- and FA-based systems that could explain the different trends in the activation energies. Nevertheless, we anticipate that this behavior could be attributed to other factors, such as the differences in the cage dynamics and dipole moments of MA (2.29 Debye⁴⁹) and FA (0.21 Debye⁴⁹) cations, which could influence the scattering of the mobile halide anions and warrants future investigations.

3. CONCLUSIONS

In summary, we have combined NMR and calorimetry measurements with DFT simulations to provide a fundamental understanding of the energetic stabilization of the “hollow” perovskites and atomistic simulation insights into the underlying ion transport in these systems, which show a strong dependence on the *en* content. From a thermodynamic point of view, FA-based “hollow” bromide perovskites are more stable compared to iodide perovskites. The least stable FAPbI₃ system gains stability upon *en* incorporation, whereas FAPbBr₃ becomes less stable. This behavior is attributed to different cage size in the bromide and iodide compounds. We find the difference in the formation enthalpy to be small, and hence it is apparent that the role of configurational entropy should be considered as a key stabilizing factor in these “hollow” perovskite structures. From *ab initio* calculations of ion migration, the FA “hollow” perovskites showed a decrease in the activation energies of the migrating halide species with increasing *en* concentration. This finding contrasts with the trend found from conductivity measurements and simulations on MAPbI₃ based “hollow” perovskites, in which the migration activation energies increase with *en* content.

ASSOCIATED CONTENT

Supporting Information

Materials and methods, synthetic details, additional figures and tables about material characterization, 1H-NMR measurements, conductivity data and DC polarization curves and time constants. Calorimetry studies and computational methods.

AUTHOR INFORMATION

Corresponding Authors

*E-mail: m-kanatzidis@northwestern.edu (Mercuri G. Kanatzidis)

*E-mail: alexandra.navrotsky@asu.edu (Alexandra Navrotsky)

*E-mail: Saiful.islam@materials.ox.ac.uk (M. Saiful Islam)

Notes

The authors declare no competing financial interest.

Acknowledgements

MGK acknowledges funding by U.S. Department of Energy, Office of Science (grant SC0012541, sample synthesis, characterization). AN, KJ, and AAV sincerely acknowledge financial support from the U.S. Department of Energy, Office of Basic Energy Sciences, Grant DE-SC0021987. MSI and NZ gratefully acknowledge an EPSRC Grant (EP/ R020485/1) and the MCC/Archer supercomputing consortium (EP/L000202/1).

References

1. Nagabhushana, G. P.; Shivaramaiah, R.; Navrotsky, A. Direct Calorimetric Verification of Thermodynamic Instability of Lead Halide Hybrid Perovskites. *Proc. Natl. Acad. Sci. U.S.A.* **2016**, *113* (28), 7717-7721.

2. Brunetti, B.; Cavallo, C.; Ciccioli, A.; Gigli, G.; Latini, A. On the Thermal and Thermodynamic (In)Stability of Methylammonium Lead Halide Perovskites. *Sci. Rep.* **2016**, *6*, 31896.
3. Ivanov, I. L.; Steparuk, A. S.; Bolyachkina, M. S.; Tsvetkov, D. S.; Safronov, A. P.; Zuev, A. Y. Thermodynamics of Formation of Hybrid Perovskite-Type Methylammonium Lead Halides. *J. Chem. Thermodyn.* **2018**, *116*, 253-258.
4. Vasileiadou, E. S.; Wang, B.; Spanopoulos, I.; Hadar, I.; Navrotsky, A.; Kanatzidis, M. G. Insight on the Stability of Thick Layers in 2D Ruddlesden–Popper and Dion–Jacobson Lead Iodide Perovskites. *J. Am. Chem. Soc.* **2021**, *143*, 6, 2523-2536.
5. Stoumpos, C. C.; Malliakas, C. D.; Kanatzidis, M. G. Semiconducting Tin and Lead Iodide Perovskites with Organic Cations: Phase Transitions, High Mobilities, and Near-Infrared Photoluminescent Properties. *Inorg. Chem.* **2013**, *52*, 15, 9019-9038.
6. Yin, W. J.; Shi, T.; Yan, Y. Unique Properties of Halide Perovskites as Possible Origins of the Superior Solar Cell Performance. *Adv. Mater.* **2014**, *26*, 4653-4658.
7. Stranks, S. D.; Eperon, G. E.; Grancini, G.; Menelaou, C.; Alcocer, M. J. P.; Leijtens, T.; Herz, L. M.; Petrozza, A.; Snaith, H. J. Electron-Hole Diffusion Lengths Exceeding 1 Micrometer in an Organometal Trihalide Perovskite Absorber. *Science*, **2013**, *342*, 341-344.
8. Stoumpos, C. C.; Kanatzidis, M. G. The Renaissance of Halide Perovskites and Their Evolution as Emerging Semiconductors. *Acc. Chem. Res.* **2015**, *48*, 10, 2791-2802.
9. Stoumpos, C. C.; Kanatzidis, M. G. Halide Perovskites: Poor Man's High-Performance Semiconductors. *Adv. Mater.* **2016**, *28*, 5778-5793.
10. Best Research-Cell Efficiencies Chart, <https://www.nrel.gov/pv/assets/pdfs/best-research-cell-efficiencies.20200925.pdf> (accessed: October **2020**).
11. Chung, I.; Lee, B.; He, J.; Chang, R. P. H.; Kanatzidis, M. G. All-Solid-State Dye-Sensitized Solar Cells with High Efficiency. *Nature*, **2012**, *485*, 486-489.
12. Kim, H-S.; Lee, C-R. Im, J-H.; Lee, K-B.; Moehl, T.; Marchioro, A.; Moon, S-J.; Humphry-Baker, R.; Yum, J-H.; Moser, J. E.; Grätzel, M.; Park, N-G. Lead Iodide Perovskite Sensitized All-Solid-State Submicron Thin Film Mesoscopic Solar Cell with Efficiency Exceeding 9%. *Sci. Rep.* **2012**, *2*, 591.

13. Park, S.; Simon, J.; Schulte, K. L.; Ptak, A. J.; Wi, J-S.; Young, D. L.; Oh, J. Germanium-on-Nothing for Epitaxial Liftoff of GaAs Solar Cells. *Joule*, **2019**, *3*, 1782-1793.
14. Metzger, W. K.; Grover, S.; Lu D.; Colegrove, E.; Moseley, J.; Perkins, C. L.; Li, X.; Mallick, R.; Zhang, W.; Malik, R.; Kephart, J.; Jiang, C-S.; Kuciauskas, D.; Albin, D. S.; Al- Jassim, M. M.; Xiong, G.; Gloeckler, M. Exceeding 20% Efficiency with *in situ* Group V Doping in Polycrystalline CdTe Solar Cells. *Nat. Energy*, **2019**, *4*, 837-845.
15. Allen, T. G.; Bullock, J.; Yang, X.; Javey, A.; De Wolf, S. Passivating Contacts for Crystalline Silicon Solar Cells. *Nat. Energy*, **2019**, *4*, 914-928.
16. Ava, T.T; Al Mamun, A.; Marsillac, S.; Namkoong, G.; A Review: Thermal Stability of Methylammonium Lead Halide-Based Perovskite Solar Cells. *Appl. Sci.* **2019**, *9*(1), 188.
17. Spanopoulos, I; Ke, W.; Kanatzidis, M. G. In Quest of Environmentally Stable Perovskite Solar Cells: A Perspective. *Helv. Chim. Acta.* **2021**, *104*, e2000173.
18. Li, N.; Niu, X.; Chen, Q.; Zhou, H. Towards Commercialization: The Operational Stability of Perovskite Solar Cells. *Chem. Soc. Rev.*, **2020**, *49*, 8235-8286.
19. Wygant, B. R.; Ye, A. Z.; Dolocan, A.; Vu, Q.; Abbot, D. M.; Mullins, C. B. Probing the Degradation Chemistry and Enhanced Stability of 2D Organolead Halide Perovskites. *J. Am. Chem. Soc.* **2019**, *141*, 45, 18170-18181.
20. Zhu, H.; Ren, Y.; Pan, L.; Ouellette, O.; Eickemeyer, F. T.; Wu, Y.; Li, X.; Wang, S.; Liu, H.; Dong, X.; Zakeeruddin, S. M.; Liu, Y.; Hagfeldt, A.; Grätzel, M. Synergistic Effect of Fluorinated Passivator and Hole Transport Dopant Enables Stable Perovskite Solar Cells with an Efficiency Near 24%. *J. Am. Chem. Soc.* **2021**, *143*, 3231-3237.
21. Chen, R.; Wang, Y.; Nie, S.; Shen, H.; Hui, Y.; Peng, J.; Wu, B.; Yin, J.; Li, J.; Zheng, N. Sulfonate-Assisted Surface Iodide Management for High-Performance Perovskite Solar Cells and Modules. *J. Am. Chem. Soc.* **2021**, *143*, 10624-10632.
22. Moller, C. K., Crystal Structure and Photoconductivity of Cesium Plumbohalides. *Nature*, **1958**, *182*, 1436.
23. Chouhan, L.; Ghimire, S.; Subrahmanyam, C.; Miyasaka, T.; Biju, V., Synthesis, Optoelectronic Properties and Applications of Halide Perovskites. *Chem. Soc. Rev.* **2020**, *49*, 2869-2885.
24. Li, Z.; Kolodziej, C.; Zhang, T.; McCleese, C.; Kovalsky, A.; Zhao, Y.; Lambrecht, W. R. L.; Burda, C. Optoelectronic Dichotomy of Mixed Halide CH₃NH₃Pb(Br_{1-x}Cl_x)₃ Single

- Crystals: Surface Versus Bulk Photoluminescence. *J. Am. Chem. Soc.* **2018**, *140*, 11811-11819.
25. Zu, F.-S.; Amsalem, P.; Salzmann, I.; Wang, R.-B.; Ralaiarisoa, M.; Kowarik, S.; Duhm, S.; Koch, N. Impact of White Light Illumination on the Electronic and Chemical Structures of Mixed Halide and Single Crystal Perovskites. *Adv. Optical. Mater.* **2017**, *5*, 1700139.
 26. Li, X.; Bi, D.; Yi, C.; Decoppet, J.-D.; Luo, J.; Zakeeruddin, S. M.; Hagfeldt, A.; Grätzel, M. A Vacuum Flash-Assisted Solution Process for High-Efficiency Large-Area Perovskite Solar Cells. *Science*, **2016**, *353*, 6294, 58-62.
 27. Jeon, N. J.; Noh, J. H.; Yang, W. S.; Kim, Y. C.; Ryu, S.; Seo, J.; Seok, S.I. Compositional Engineering of Perovskite Materials for High-Performance Solar Cells. *Nature*, **2015**, *517*, 476-480.
 28. Fabiani, D. H.; Stoumpos, C. C.; Laurita, G.; Kaltzoglou, A.; Kontos, A. G.; Falaras, P.; Kanatzidis, M. G. Seshadri, R. Reentrant Structural and Optical Properties and Large Positive Thermal Expansion in Perovskite Formamidinium Lead Iodide. *Angew. Chem. Int. Ed.* **2016**, *55*, 15392-15396.
 29. Whitfield, P. S.; Herron, N.; Guise, W. E.; Page, K.; Cheng, Y. Q.; Milas, I.; Crawford. Structures, Phase Transitions and Tricritical Behavior of the Hybrid Perovskite Methyl Ammonium Lead Iodide. *Sci. Rep.* **2016**, *6*, 35685.
 30. Ono, L. K.; Juarez-Perez, E. J.; Qi, Y. Progress on Perovskite Materials and Solar Cells with Mixed Cations and Halide Anions. *ACS Appl. Mater. Interfaces*, **2017**, *9*, 30197-30246.
 31. Jiang, S.; Luan, Y.; Jang, J. I.; Baikie, T.; Huang, X.; Li, R.; Saouma, F. O.; Wang, Z.; White, T. J.; Fang, J. Phase Transitions of Formamidinium Lead Iodide Perovskite Under Pressure. *J. Am. Chem. Soc.* **2018**, *140*, 42, 13952-13957.
 32. Park, B.-W.; Seok, S.I. Intrinsic Instability of Inorganic–Organic Hybrid Halide Perovskite Materials. *Adv. Mater.* **2019**, *31*, 1805337.
 33. Brennan, M. C.; Draguta, S.; Kamat, P. V.; Kuno, M. Light-Induced Anion Phase Segregation in Mixed Halide Perovskites. *ACS Energy Lett.* **2018**, *3*, 1, 204-213.
 34. McMeekin, D. P.; Sadoughi, G.; Rehman, W.; Eperon, G. E.; Saliba, M.; Hörantner, M. T.; Haghighirad, A.; Sakai, N.; Korte, L.; Rech, B.; Johnston, M. B.; Herz, L. M.; Snaith, H. J. A Mixed-Cation Lead Mixed-Halide Perovskite Absorber for Tandem Solar Cells.

Science **2016**, *351*, 151-155.

- 35.** Chen, W.; Li, W.; Gan, Z.; Cheng, Y.-B.; Jia, B.; Wen, X. Long-Distance Ionic Diffusion in Cesium Lead Mixed Halide Perovskite Induced by Focused Illumination. *Chem. Mater.* **2019**, *31*, 21, 9049-9056.
- 36.** Ke, W.; Stoumpos, C. C.; Zhu, M.; Mao, L.; Spanopoulos, I.; Liu, J.; Kontsevoi, O. Y.; Chen, M.; Sarma, D.; Zhang, Y.; Wasielewski, M. R.; Kanatzidis, M. G. Enhanced Photovoltaic Performance and Stability with a New Type of “Hollow” 3D Perovskite $\{en\}FASnI_3$. *Sci. Adv.* **2017**, *3*, e1701293.
- 37.** Senocrate, A.; Spanopoulos, I.; Zibouche, N.; Maier, J.; Islam, M. S.; Kanatzidis, M. G. Tuning Ionic and Electronic Conductivities in the “Hollow” Perovskite $\{en\}MAPbI_3$. *Chem. Mater.* **2021**, *33*, 2, 719-726.
- 38.** Spanopoulos, I.; Ke, W.; Stoumpos, C. C.; Schueller, E.C.; Kontsevoi, O. Y.; Seshadri, R.; Kanatzidis, M. G. Unraveling the Chemical Nature of the 3D “Hollow” Hybrid Halide Perovskites. *J. Am. Chem. Soc.* **2018**, *140*, 17, 5728-5742.
- 39.** Spanopoulos, I.; Hadar, I.; Ke, W.; Guo, P.; Mozur, E.V.; Morgan, E.; Wang, S.; Zheng, D.; Padgaonkar, S.; Reddy, G. N. M.; Weiss, E.A.; Hersam, M. C.; Seshadri, R.; Schaller, R. D.; Kanatzidis, M. G. Tunable Broad Light Emission from 3D “Hollow” Bromide Perovskites Through Defect Engineering. *J. Am. Chem. Soc.* **2021**, *143*, 18, 7069-7080.
- 40.** Goldschmidt, V. M. Die Gesetze der Krystallochemie. *Naturwissenschaften*, **1926**, *14*, 477.
- 41.** Kubicki, D. J.; Prochowicz, D.; Hofstetter, A.; Saski, M.; Yadav, P.; Bi, D.; Pellet, N.; Lewiński, J.; Zakeeruddin, S. M.; Grätzel, M.; Emsley, L. Formation of Stable Mixed Guanidinium–Methylammonium Phases with Exceptionally Long Carrier Lifetimes for High-Efficiency Lead Iodide-Based Perovskite Photovoltaics. *J. Am. Chem. Soc.* **2018**, *140*, 9, 3345–3351
- 42.** Yi, C.; Luo, J.; Meloni, S.; Boziki, A.; Ashari-Astani, N.; Grätzel, C.; Zakeeruddin, S. M.; Röthlisberger, U.; Grätzel, M. Entropic stabilization of mixed A-cation ABX_3 metal halide perovskites for high performance perovskite solar cells. *Energy Environ. Sci.*, **2016**, *9*, 656-662.
- 43.** Ünlü, F.; Jung, E.; Öz, S.; Choi, H.; Fischer, T.; Mathur, S. Chemical Processing of Mixed-Cation Hybrid Perovskites: Stabilizing Effects of Configurational Entropy. In *Perovskites Solar Cells: Materials, Processes, and Devices*, John Wiley and Sons, **2015**, pp 1-31.

44. Saliba, M.; Matsui, T.; Seo, J.Y.; Domanski, K.; Correa-Baena, J-P.; Nazeeruddin, M. K.; Zakeeruddin, S. M.; Tress, W.; Abate, A.; Hagfeldt, A.; Grätzel, M. Cesium-containing triple cation perovskite solar cells: improved stability, reproducibility and high efficiency. *Energy Environ. Sci.*, **2016**, *9*, 1989–1997
45. Eames, C.; Frost, J. M.; Barnes, P. R. F.; O'Regan, B. C.; Walsh, A.; Islam, M. S. Ionic Transport in Hybrid Lead Iodide Perovskite Solar Cells. *Nat. Commun.* **2015**, *6*, 7497.
46. Ferdani, D. W.; Pering, S. R.; Ghosh, D.; Kubiak, P.; Walker, A. B, Lewis, S. E.; Johnson, A. L.; Baker, P. J.; Islam, A. S.; Cameron, P. J. Partial Cation Substitution Reduces Iodide Ion Transport in Lead Iodide Perovskite Solar Cells. *Energy Environ. Sci.* **2019**, *12*, 2264-2272.
47. Zibouche, N.; Islam, M. S. Structure–Electronic Property Relationships of 2D Ruddlesden–Popper Tin- and Lead-Based Iodide Perovskites. *ACS Appl. Mater. Interface*, **2020**, *12*, 13, 15328-15337.
48. Ghosh, D.; Smith, A. R.; Walker, A. B.; Islam, M. S. Mixed A-Cation Perovskites for Solar Cells: Atomic-Scale Insights into Structural Distortion, Hydrogen Bonding, And Electronic Properties. *Chem. Mater.* **2018**, *30*, 15, 5194-5204.
49. Gets, D. S.; Verkhogliadov, G. A.; Danilovskiy, E. Y.; Baranov, A. I.; Makarov, S. V.; Zakhidov, A. A. Dipolar Cation Accumulation at the Interfaces of Perovskite Light-Emitting Solar Cells. *J. Mater. Chem. C.* **2020**, *8*, 16992-16999.

FIGURES AND TABLES

Table 1. Thermochemical cycle to calculate the formation enthalpies of the $(A)_{1-x}(en)_x(Pb)_{1-0.7x}(X)_{3-0.4x}$ “hollow” perovskites.

$(A)_{1-x}(en)_x(Pb)_{1-0.7x}(X)_{3-0.4x}(s) \rightarrow 1-x(AX)_{(sln)} + x(enX_2)_{(sln)} + 1-0.7x(PbX_2)_{(sln)}$	$\Delta H_1 = \Delta H_{ds} (A)_{1-x}(en)_x(Pb)_{1-0.7x}(X)_{3-0.4x}$
$AX (s) \rightarrow AX (sln)$	$\Delta H_2 = \Delta H_{ds} (AX)$
$enX_2 (s) \rightarrow enX_2(sln)$	$\Delta H_3 = \Delta H_{ds} (enX_2)$
$PbX_2 (s) \rightarrow PbX_2(sln)$	$\Delta H_4 = \Delta H_{ds} (PbX_2)$
$(1-x)(AX)_{(s)} + x(enX_2)_{(s)} + (1-0.7x)(PbX_2)_{(s)} \rightarrow (A)_{1-x}(en)_x(Pb)_{1-0.7x}(X)_{3-0.4x}(s)$	$\Delta H_5 = \Delta H_f^\circ (A)_{1-x}(en)_x(Pb)_{1-0.7x}(X)_{3-0.4x}$
$\Delta H_5 = -\Delta H_1 + (1-x) \Delta H_2 + x\Delta H_3 + (1-0.7x) \Delta H_4$	

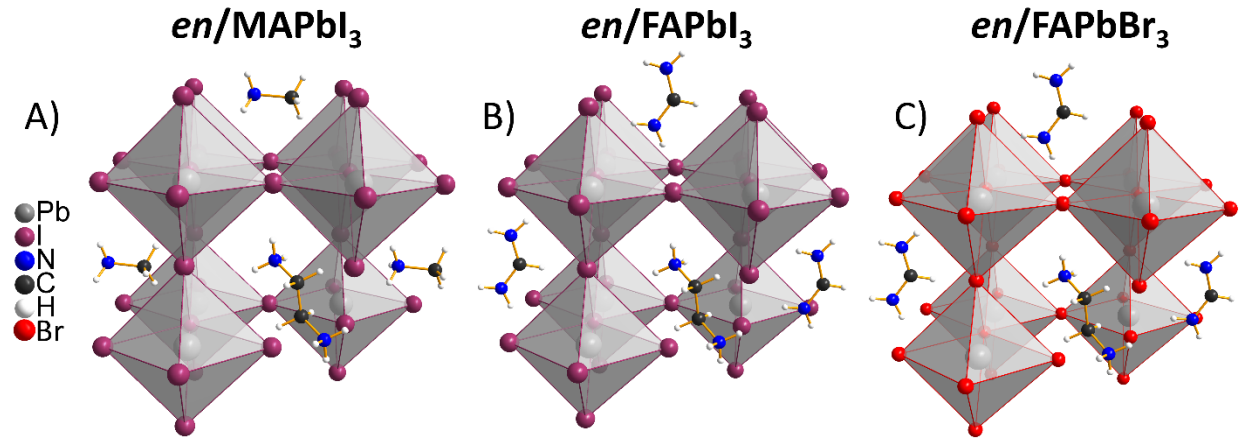


Figure 1. Hypothetical crystal structures of the 3D “hollow” A) $en/MAPbI_3$, B) $en/FAPbI_3$, and C) $en/FAPbBr_3$ perovskites.

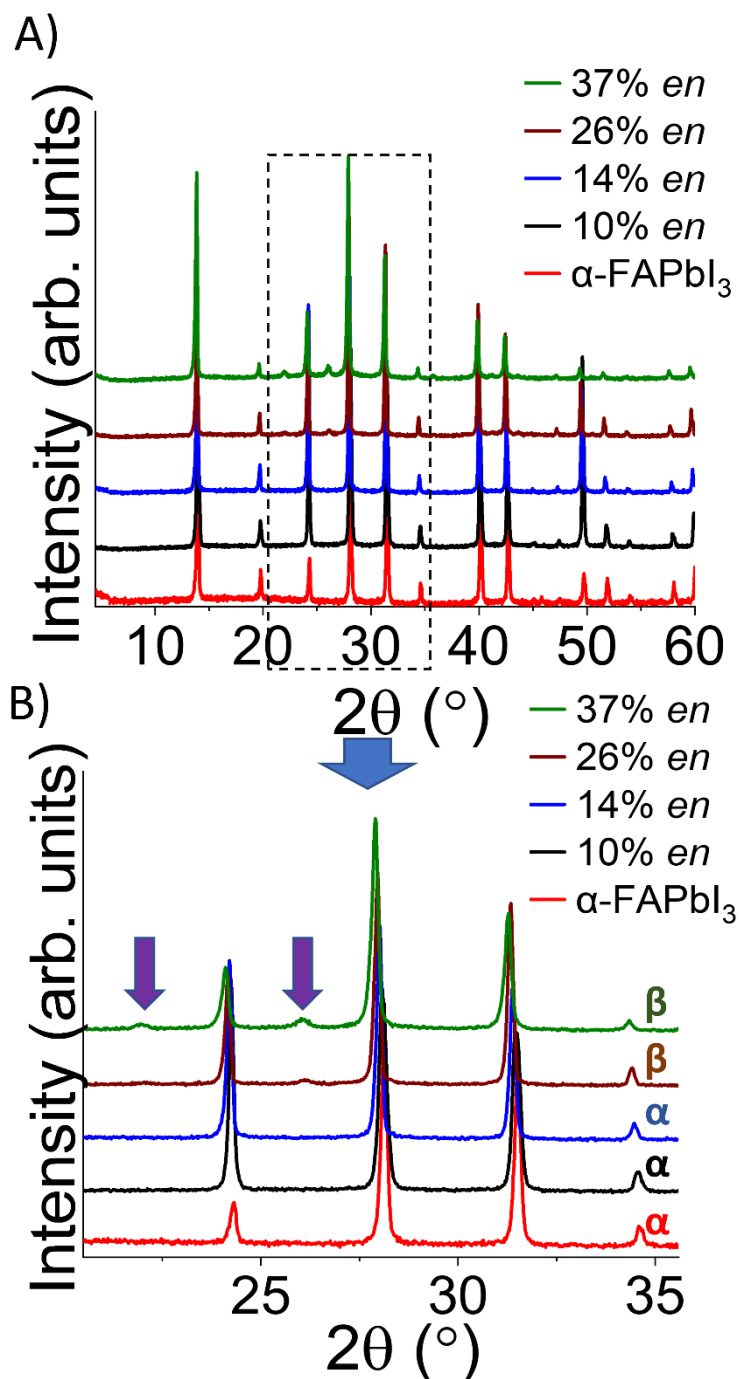


Figure 2. PXRD patterns of $(\text{FA})_{1-x}(\text{en})_x(\text{Pb})_{1-0.7x}(\text{I})_{3-0.4x}$ perovskites with increasing amounts of *en* dication. The resulting materials for *x* values up to 14% are isostructural to the pristine α -phase FAPbI_3 , while the rest of the hollow material for *x* values above 26% are isostructural to the pristine β -phase FAPbI_3 . The additional diffraction peaks at $2\theta = 22.3^\circ$ and 26.4° are characteristic peaks of the pure β -phase FAPbI_3 .

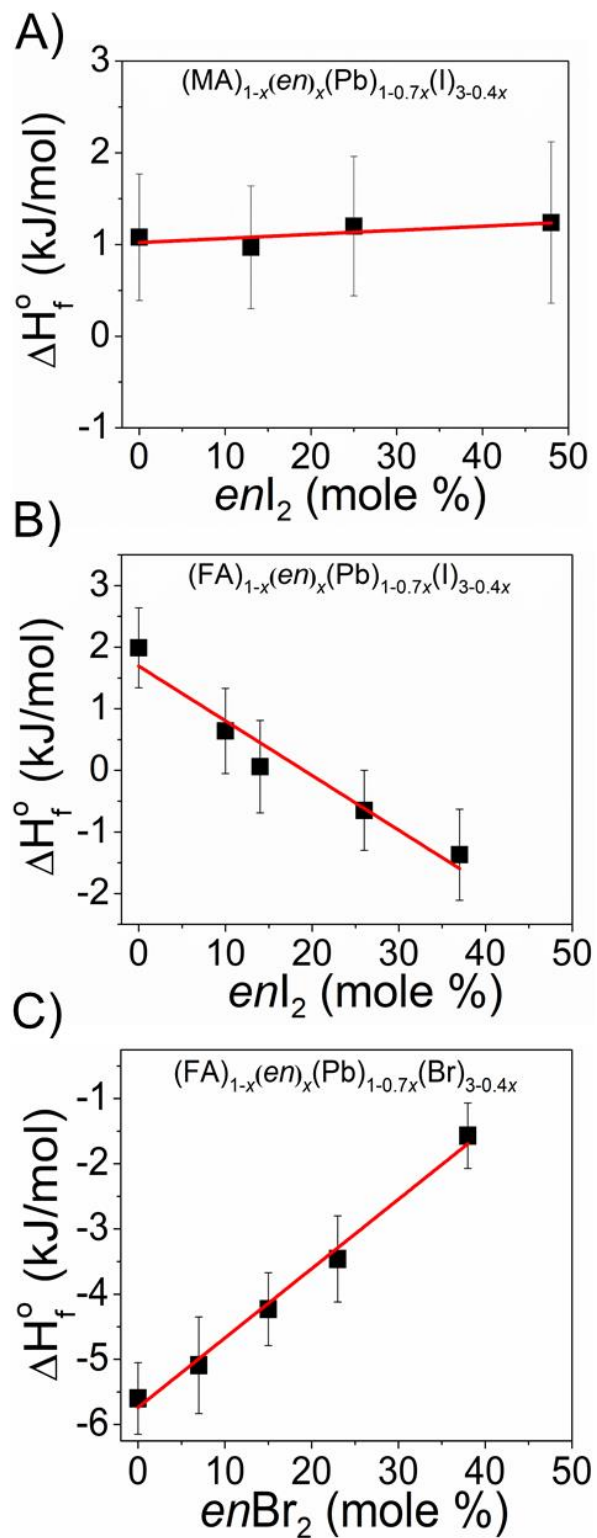


Figure 3. Formation enthalpy (ΔH_f°) as a function of mol % enX_2 for the A) $(MA)_{1-x}(en)_x(Pb)_{1-0.7x}(I)_{3-0.4x}$, B) $(FA)_{1-x}(en)_x(Pb)_{1-0.7x}(I)_{3-0.4x}$, and C) $(FA)_{1-x}(en)_x(Pb)_{1-0.7x}(Br)_{3-0.4x}$ “hollow” perovskites.

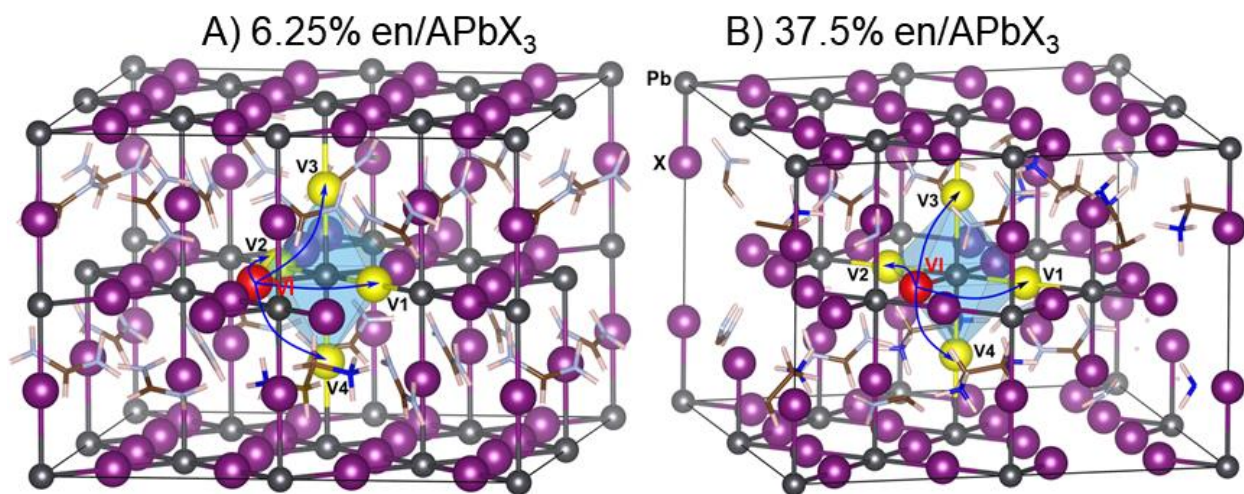


Figure 4. Simulated crystal structures of %*en*FAPbX₃ and ion migration paths for *en* content of A) 6.25% and B) 37.5%. X (= I, Br) Anion migration pathways are indicated by the arrows between the initial X halide vacancy position VI (red) and the final nonequivalent halide vacancy positions (yellow marked as V1, V2, V3, and V4).